PTEP

Prog. Theor. Exp. Phys. **2020**, 073I02 (23 pages)
DOI: 10.1093/ptep/ptaa091

A classical density functional theory model for fragility in the hard-sphere limit

Arijit Mondal and Shankar P. Das*

School of Physical Sciences, Jawaharlal Nehru University, New Delhi 110067, India
*E-mail: shankar@jnu.ac.in

Received February 1, 2020; Revised May 5, 2020; Accepted May 27, 2020; Published July 28, 2020

We study, using the classical density functional theory (DFT), the fragility and short-time elastic constants of a soft-sphere liquid. For the amorphous state, the order parameter is the inhomogeneous density function $\rho(\mathbf{r})$ which is described in terms of Gaussian density profiles centered on a set random lattice points $\{\mathbf{R}_i\}$. The latter is characterized in terms of the Bernel pair function $g_{\rm B}(r)$. Based on the Adam–Gibbs-type relation between the α relaxation time τ_α and the configurational entropy $\mathcal{S}_{\rm c}$, a thermodynamic fragility $m_{\rm T}$ for the liquid is defined. The concentration or average density of the liquid is treated as the control parameter here instead of temperature. The configurational entropy of the liquid is calculated using the DFT model. Variations in the short-range structure of the amorphous state are made with different choices for the value of $g_{\rm B}(r)$ at short distances, and its implications on the correlation between fragility $m_{\rm T}$ and the softness index n are studied. The dependence of Poisson's ratio ν on the softness index n of the interaction potential is also obtained from the density dependence of the metastable state free energy. The correlation between $m_{\rm T}$ and ν follows.

Subject Index I00, I01, I02

1. Introduction

The ergodic state of a liquid is characterized by the characteristic relaxation times for fluctuations around an equilibrium state. The fragility index of a glass-forming liquid is related to the final relaxation process near the glass transition point. A generic feature of the supercooled liquid state is the rapid increase of its relaxation time $\tau_\alpha(T)$. The nature of this dependence is demonstrated with the Angell plot [1], which presents $\ln[\tau_\alpha(T)/\tau_0]$ vs. $x = T_{\rm g}/T$ for different materials. Here, τ_0 is a characteristic time scale of the dynamics at high temperatures, and $T_{\rm g}$ is the so called calorimetric glass transition temperature. The latter is defined as a characteristic property for the glass-forming liquid through the relation

$$\log\left[\frac{\tau}{\tau_0}\right]_{T=T_{\rm g}} = \mathcal{B}, \tag{1}$$

where $\mathcal{B}$ is a chosen number. For molecular glasses it is taken as 16. The Angell plot has been used in the classification of various glass-forming systems as being strong and fragile [2,3]. Materials in which a uniform increase of relaxation time is seen over temperatures ranging from high to deep below the freezing point are termed strong liquids, e.g. B_2O_3 or SiO_2. In the other limit, crossover in the temperature dependence of the viscosity or relaxation times is observed for fragile liquids. For

glass-forming materials, this property is quantified in terms of a corresponding fragility parameter m which is the slope of the viscosity–temperature curve at $T = T_g$:

$$m = \left.\frac{d \ln \tau}{dx}\right|_{x=1}. \tag{2}$$

For example, $m = 81$ for o-terphenyl and $m = 20$ for SiO_2 illustrate two extreme cases of fragile and strong systems. The above-described characteristic features of glassy dynamics for a molecular system have also been observed in the relaxation behavior of colloidal suspensions [4–6]. In this case the fragility and glass transition points are defined in terms of the density or concentration of the particles, similar to the definition of Eq. (1) in terms of temperature. We have the glass transition point at concentration η_g. For $\mathcal{B} = 5$ a figure similar to the Angell plot was obtained [7] for soft matter of deformable spheres.

The elastic response of a supercooled liquid approaching glass transition signifies a solid-like behavior. In general, even a fluid much above its freezing point produces an elastic response over very short time scales. The high-frequency elastic constants are expressed in terms of the interaction potential $u(r)$ between the fluid particles. To calculate these elastic coefficients for a liquid we apply the model of Zwanzig and Mountain [8–10]. This is a microscopic approach in which the elastic constants are obtained in terms of frequency-dependent viscosities for the system. These generalized memory functions are written in terms of Greek–Kubo-type relations [11]. A full calculation of the dynamics is avoided here since it is only the short-time or high-frequency elastic constant which is computed. The final results are therefore obtained in terms of equal-time correlation functions. For two-body interaction potentials this is simply the pair correlation functions $g(r)$.

It is well known that the dynamics of a dense liquid is strongly affected by its structural properties [12], which are determined by the interaction potentials between its constituent particles. In confirmation of this dependence the α relaxation time scale for long-time dynamics has been linked with the configurational entropy $\mathcal{S}_c$ of a glassy system [13] through an Adam–Gibbs-like relation [14]. Following this link, a thermodynamic fragility index m_T is obtained in terms of $\mathcal{S}_c$, analogous to the usual kinetic fragility [1] obtained from relaxation behavior. For calculating $\mathcal{S}_c$ we use here the classical density functional theory (DFT) [15–18]. The DFT model requires the following two basic inputs:

(a) The static correlations of the uniform liquid state. These are obtained in terms of the basic interaction potential $u(r)$ between the fluid particles.
(b) The solid-like structure for the amorphous metastable state. This is realized with a suitable choice for the inhomogeneous density function $\rho(\mathbf{r})$ in terms of Gaussian density profiles centered around a set of points $\{\mathbf{R}_i\}$ forming an amorphous structure.

For part (a) above, we will consider here a purely repulsive soft-sphere potential for the particles:

$$u(r) = \epsilon_0 \left(\frac{\sigma}{r}\right)^n. \tag{3}$$

The configurational entropy $\mathcal{S}_c$, and hence the thermodynamic fragility for the metastable state, is sensitive to this underlying structure $\{\mathbf{R}_i\}$ used to describe the corresponding heterogeneous density distribution in part (b). In the present work we study the role of this short-range structure on the correlation between high-frequency elastic response and the thermodynamic fragility m_T for the metastable liquid. The average density ρ_0 is expressed in terms of the dimensionless parameter

$\eta = \pi\rho_0\sigma^3/6$. The quantity σ is a basic length scale associated with the two-particle interaction given in Eq. (3). For the hard-sphere system, σ is the hard-sphere diameter and η is the packing fraction. We study how the softness index n in Eq. (3) correlates with the corresponding thermodynamic fragility index $m_{\rm T}$, as well as the ratio of short-time elastic coefficients for the liquid. The dependence of the fragility on the interaction potential approaching the hard-sphere limit is also obtained from the extrapolation of our results.

The paper is organized as follows: In Sect. 2, we describe the basic properties for the supercooled liquids we study in this work. In Sect. 3 we focus on classical DFT and discuss the necessary inputs for the calculation, with some of the details being presented in the appendices. We present here how the metastable states of a liquid with inhomogeneous density distributions are identified as local minima of the free energy functional. We describe the scheme for calculation of thermodynamic fragility using results for configurational entropy and its density dependence. We also present in this section the model equations used for computation of the short-time elastic constants. In Sect. 4 we present the numerical results obtained. This includes how of the fragility index $m_{\rm T}$ depends on the soft-sphere interaction potential exponent n. The relation between dynamic and elastic properties is also presented here. We end the paper with a discussion of the results.

2. Fragility and elasticity

In this section we describe very briefly the basic quantities of interest in this study and discuss the methods used for calculating these.

2.1. Thermodynamic fragility

We first illustrate how the thermodynamic fragility of a glass-forming system is directly linked to its configurational entropy. The idea of thermodynamic fragility is based on the generally accepted link between relaxation time τ and configurational entropy $\mathcal{S}_{\rm c}$ [19] in a supercooled liquid. This is similar to the Adam–Gibbs-type relation originally proposed for polymeric systems [14]:

$$\tau \sim \tau_0 \exp\left[\frac{\eta}{\mathcal{S}_{\rm c}}\right]. \tag{4}$$

Hence, the relaxation time $\tau \to \infty$ as $\mathcal{S}_{\rm c} \to 0$. The Kauzmann point $\eta_{\rm K}$ represents an ultimate point such that as $\eta \to \eta_{\rm K}$, the configurational entropy $\mathcal{S}_{\rm c} \to 0$. The packing at this Kauzmann point, $\eta_{\rm K}$, is obtained by doing a fit of $\mathcal{S}_{\rm c}(\eta)$ for $\eta < \eta_{\rm K}$ with the simple form

$$\mathcal{S}_{\rm c} = \mathcal{S}_0(\eta_{\rm K} - \eta)^a. \tag{5}$$

The configurational entropy $\mathcal{S}_{\rm c}$, calculated using the density functional model, is fitted with the form in Eq. (5), and the exponent a is generally less than unity. The $\mathcal{S}_{\rm c}(\eta)$ vs. η relation is useful in estimating the thermodynamic fragility $m_{\rm T}$. To see this connection, consider the relaxation time τ/τ_0 being expressed as a function of η. By taking the derivative with respect to $\Delta = \eta/\eta_{\rm g}$, analogous to the case of kinetic fragility m [20–23], we define the thermodynamic fragility:

$$m_{\rm T} \sim \frac{d}{d\Delta}\ln\left[\frac{\tau}{\tau_0}\right]\bigg|_{\Delta=1} = \frac{1}{\mathcal{S}_{\rm c}(\eta_{\rm g})}\left[1 + \frac{a}{\Delta_{\rm K} - 1}\right]. \tag{6}$$

The quantity $\Delta_{\rm K}$ is defined as $\Delta_{\rm K} = \eta_{\rm K}/\eta_{\rm g}$. We estimate the thermodynamic fragility $m_{\rm T}$ by evaluating the right-hand side of Eq. (6). We also need the glass transition point $\eta_{\rm g}$ to calculate $m_{\rm T}$.

At the so-called glass transition point η_g we have, from Eq. (4),

$$\frac{\eta}{\mathcal{S}_c}\Big|_{\eta=\eta_g} = \ln\left[\frac{\tau}{\tau_0}\right]_{\eta=\eta_g} = \frac{1}{a_0}, \tag{7}$$

where $a_0^{-1} = \mathcal{B}\ln(10)$. Equation (7) is useful for computing η_g for the liquid. Next, we consider the calculation of the high-frequency elastic response.

2.2. The short-time elastic constants

The high-frequency or short-time response of the isotropic metastable liquid is obtained in terms of the corresponding elastic constants K_∞ and G_∞ and thermodynamics pressure P. In the following we express these three thermodynamic quantities in units of $\rho_0 k_B T$, where ρ_0 is the equilibrium density and T is the temperature. Following the model of Mountain and Zwanzig [8,9], we write

$$G_\infty = 1 + \frac{4\eta}{5}\int_0^\infty dr g(r)\frac{d}{dr}\left[r^4\frac{du}{dr}\right], \tag{8}$$

$$K_\infty = \frac{2}{3} + P + \frac{4\eta}{3}\int_0^\infty dr g(r) r^3\frac{d}{dr}\left[r\frac{du}{dr}\right], \tag{9}$$

$$P = 1 - 4\eta\int_0^\infty dr g(r) r^3\frac{du}{dr}. \tag{10}$$

In writing the above relations in a dimensionless form we scale length with the microscopic scale σ of the interaction potential. The three quantities K_∞, G_∞, and P are related through the linear relation

$$K_\infty = \frac{5}{3}G_\infty + 2(P-1). \tag{11}$$

3. The density functional model

In the present work we consider an inhomogeneous metastable liquid for which the free energy is obtained using the classical density functional model. In DFT, the free energy of the liquid is expressed as a functional of the inhomogeneous density $\rho(\mathbf{x})$, which is treated as an order parameter for the supercooled state. The inhomogeneous density $\rho(\mathbf{x})$ is expressed as a sum of Gaussian density profiles centered on the random lattice structure $\{\mathbf{R}_i\}$. The standard parametric form of $\rho(\mathbf{x})$ used in the present work is

$$\rho(\mathbf{r}) = \sum_{i=1}^{N}\left(\frac{\alpha}{\pi}\right)^{\frac{3}{2}} e^{-\alpha|\mathbf{r}-\mathbf{R_i}|^2}. \tag{12}$$

Here, α is the width parameter for the Gaussian density profiles, and is assumed to be the same for all points on $\{\mathbf{R}_i\}$. The equilibrium free energy is obtained by identifying the corresponding width parameter $\alpha = \alpha_{\min}$ at which the free energy is a minimum. The total free energy f per particle is expressed as a sum of two parts,

$$f[\rho(\mathbf{x})] = f_{id}[\rho(\mathbf{x})] + f_{ex}[\rho(\mathbf{x})]. \tag{13}$$

The ideal part of the free energy f_{id} involves the entropic contribution for the noninteracting system [24], while the excess part f_{ex} includes the role of interactions. In simple DFT the quantity $f_{ex}[\rho(\mathbf{x})]$

is expressed in a low-order functional Taylor expansion in terms of density fluctuations $\delta\rho(\mathbf{x}) = \rho(\mathbf{x}) - \rho_0$, around an average density ρ_0 for the uniform state [25–28]. However, with sharply localized density distributions (corresponding to large values of $\alpha\sigma^2$ in Eq. (12) for the inhomogeneous density), the fluctuations are large and a bare functional expansion in terms of $\delta\rho(\mathbf{x})$ proves to be inadequate. The excess part $f_{\rm ex}$ is therefore calculated using an effective medium approach referred to as the modified weighted density approximation (MWDA) [29–31]. The procedure is standard and is sketched briefly in the next section and Appendix A. As already discussed in the introduction, the calculation of $f_{\rm ex}$ with this approach requires two key inputs, namely a structural description of the uniform density homogeneous liquid, and also for the amorphous state with inhomogeneous density. In the following we will discuss how we implement these two inputs in our calculation.

3.1. The homogeneous liquid: soft-sphere interaction

In classical DFT, the free energy of the inhomogeneous state is therefore calculated using the corresponding uniform liquid state as a reference. The functional Taylor series expansion for the excess free energy $f_{\rm ex}[\rho(\mathbf{x})]$ in terms of fluctuation of $\delta\rho(\mathbf{x})$ involves, at the lowest order, the Ornstein–Zernike [32] direct correlation functions $c(r;\rho_0)$ of the uniform liquid of density ρ_0. In the present calculation for the soft-sphere potential, the corresponding $c(r;\rho_0)$ is calculated using the Bridge function method. The structural properties for the homogeneous liquid in which the constituents are interacting through two-body potential $u(r)$ are primarily represented in terms of the pair function $g(r)$. To calculate these structural properties like $c(r)$ or $g(r)$ of the homogeneous liquid with soft-sphere interaction, we represent the system in terms of an equivalent hard-sphere liquid. The equivalent hard-sphere diameter d_n is determined by imposing that the free energies of the actual and equivalent systems match to linear order in fluctuations. This gives rise to the standard Barker–Henderson [32,33] formula:

$$d_n = \int_0^\infty dr(1 - e^{-\beta u(r)}). \tag{14}$$

In the present case, $u(r)$ is the repulsive soft-sphere potential of Eq. (3). Here, the diameter d_n depends on the inverse temperature (β) and also on the index n for the soft-sphere potential [34]. In Fig. 1 we show the equivalent hard-sphere diameter d_n vs. the index n characterizing the soft-sphere potential defined in Eq. (3) corresponding to $(k_{\rm B}T/\epsilon_0) = \beta^{-1} = 2.0$.

There are different methods for computing the pair function for a hard-sphere liquid using integral equation approaches [32]. Here, this is computed using the Bridge function method of Rogers and Young [35,36]. The argument r of $g(r)$ is expressed in units of a characteristic microscopic length, generally associated with the interaction potential. This is σ for the soft-sphere potential of Eq. (3) in the present case. The function $g(r)$ also depends on the softness parameter n for the potential, and the average density ρ_0 for the fluid ($\eta = \pi\rho_0\sigma^3/6$). Figure 2 shows the pair function $g(r/\sigma)$ for $\eta = 0.523$ corresponding to interaction potentials with indices $n = 25$, 30, 35, and 60. The inset shows how the position of the respective first peak of $g(r/\sigma)$ changes with n. With the pair correlation function, the corresponding $c(r)$ is also obtained through the Ornstein–Zernike relation.

3.2. Structural input for the DFT

In DFT calculations, an average description of the corresponding density distribution characterizing this inhomogeneous state is required as an input. This is similar to the case of a crystal for which a

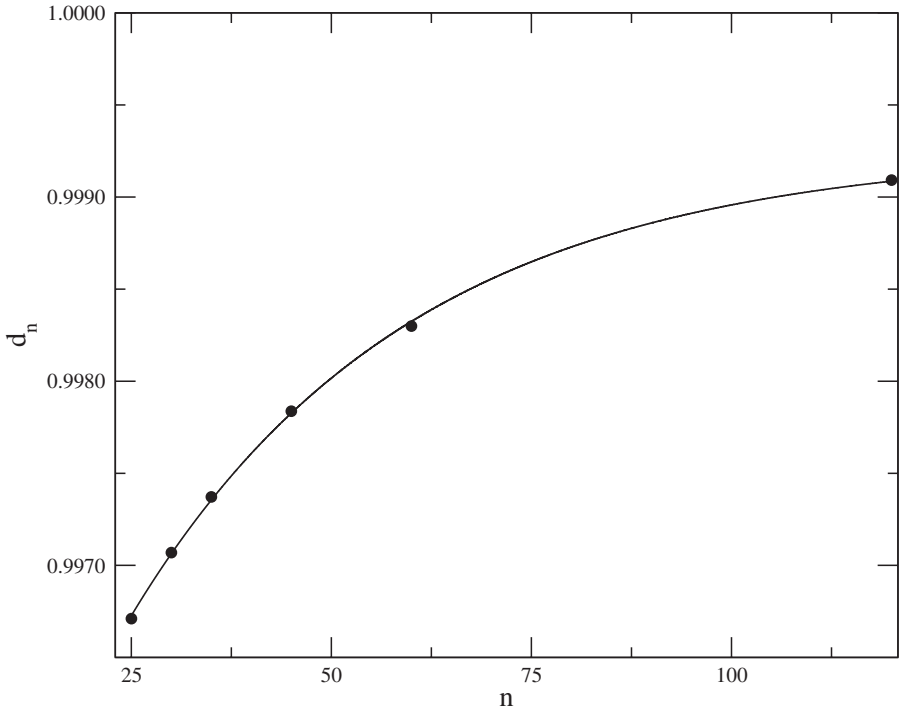

Fig. 1. The diameter of the equivalent hard-sphere system in units of σ vs. softness index n at $\beta = 0.5$.

suitably chosen lattice with long-range order characterizes the corresponding inhomogeneous density distribution. The DFT approach does not explain spontaneous breaking of the isotropic symmetry in the homogeneous liquid; rather, it allows one to identify the crystal symmetry in the inhomogeneous state by picking up the appropriate density function $\rho(\mathbf{x})$, which is then tested to find a minimum of the free energy functional. In the present context of the glassy state, Gaussian density profiles are taken to be centered on an amorphous lattice $\{\mathbf{R}_i\}$. Averages of physical properties over different choices of lattice $\{\mathbf{R}_i\}$ are expressed in terms of a corresponding radial distribution function $w(r, n)$. For the isotropic system we consider here, the pair function depends on the radial distance r as well as the parameter n of the soft-sphere interaction. This pair function describing the distribution of $\{\mathbf{R}_i\}$ also depends on the average density η for the liquid state. This η dependence of $w(r, n)$ is not shown here to avoid clutter. We model this distribution function $w(r, n)$ characterizing the metastable state for the soft-sphere liquid (with softness index n) with average density η in terms of the Bernal pair function $g_{\rm B}(R)$ [37,38] for a system of randomly packed hard spheres. The argument R here denotes distance scaled by the diameter d_n of the spheres. We incorporate the n and η dependence of the function $w(r)$ in terms of $g_{\rm B}(R)$ through the scaling relation [38,39]

$$w(r, n) = g_{\rm B}\left[\tilde{r}\left(\frac{\eta}{\eta_0}\right)^{1/3}\right]. \tag{15}$$

The Bernal function $g_{\rm B}(R)$ is constructed using the Bennett algorithm [40]. The n dependence is present on the right-hand side of Eq. (15) in terms of the scaled length scale $\tilde{r} = r/d_n$ in units of the corresponding equivalent hard-sphere diameter d_n given in Eq. (14). The density dependence on the right-hand side of Eq. (15) is present with respect to the chosen parameter η_0. On scaling the argument r of the pair function $w(r, n)$, the argument of $g_{\rm B}$ changes to $\tilde{r}(\eta/\eta_0)^{1/3}$, making the structure more scaled out compared to the hard-sphere case since $\eta_0 \geq \eta$.

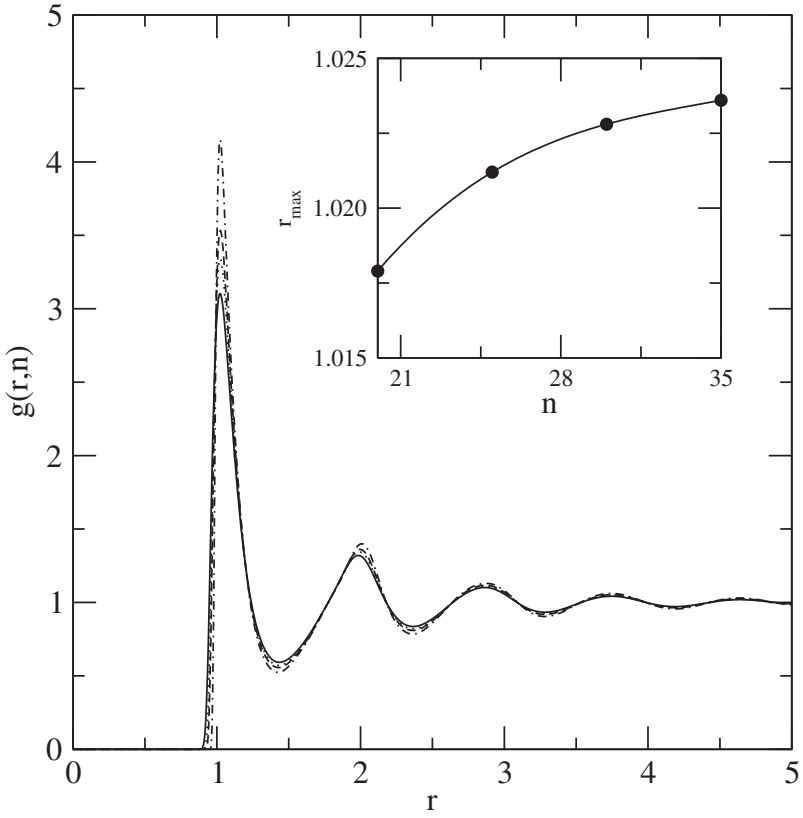

Fig. 2. $g(r/\sigma)$ vs. r/σ for different values of the soft-sphere potential index $n = 25$ (solid), 30 (dotted), 35 (dashed), and 60 (dot-dashed). The density is $\eta = 0.523$. The inset shows the height of the first peak in $g(r)$ vs. n.

It has been known from earlier DFT calculations [28,31] with hard-sphere systems that a key factor in minimizing the free energy is the corresponding value of $g_{\rm B}(1)$ at contact being used in the model. To study the soft-sphere system we treat the corresponding property of the structure function $w(r, n)$ as an independent parameter characterizing the metastable structure, and make it explicitly dependent on the softness index n of interaction potential, as well as the average density η. This contact value of the structure function $w(r, n)$ in particular relates to the short-range density distributions in the amorphous state. We model its n and η dependence, i.e. $w_{\rm c}(n)\equiv w(1, n)$, for the soft-sphere system borrowing from the results for $g(1, n)$ of the corresponding uniform system having the same interaction potential as Eq. (3) and the same density η:

$$w_{\rm c}(n)\equiv w(1,n) = g_{\rm B}(1)\left[1 + c_0\left\{\frac{g(1,n)}{g(1,\infty)} - 1\right\}\right], \tag{16}$$

where c_0 is treated as an adjustable parameter. The contact function $g(1, n)$ for the uniform system is obtained using the Bridge function method. In the hard-sphere case, i.e. for the $n \to \infty$ limit, the above prescription for $w_{\rm c}(n)$ reduces to the corresponding result $g_{\rm B}(1)$ for the Bernel function [28,31]. To summarize, the structure function $w(r, n)$ used in averaging over a corresponding amorphous lattice $\{\mathbf{R}_i\}$ is modelled here using Eqs. (15), and its contact value is specifically chosen as given in Eq. (16). This is an important ingredient in calculating the free energy of the inhomogeneous state, and hence for the calculation of the configurational entropy of this state as well.

To calculate the free energy $f_{\rm ex}$ using MWDA, the strongly inhomogeneous amorphous solid-like state is replaced by an effective liquid of uniform density $\hat{\eta}$. The latter is obtained from the solution of the integral equations in Eqs. (A.4) and (A.5), following the procedures briefly discussed in Appendix A. Generally, $\hat{\eta}$ has a much lower value than η and hence the free energy of the effective liquid is obtained using standard formulas for the liquid state. The integral equations for the concentration $\hat{\eta}$ of the equivalent liquid involve taking an average over different realizations of the $\{\mathbf{R}_i\}$ and are implemented with the structure function $w(r)$. The metastable state of the liquid is identified with a local minimum of the free energy with respect to variation of the width parameter α for the density profiles defined in Eq. (12). Next, the configurational entropy $\mathcal{S}_{\rm c}$ for this metastable state is calculated. For this, we need to obtain the total free energy f and also identify its vibrational part $f_{\rm vib}$. In Appendix B we outline how the configurational entropy $\mathcal{S}_{\rm c}$ is obtained using density functional theory.

3.3. Elastic constants

The free energy of the inhomogeneous solid in the metastable state is calculated using MWDA, and this result becomes an important ingredient in the calculation of the elastic constants for the inhomogeneous state. We consider the short-time or high-frequency elastic response of the system. In the inhomogeneous metastable state identified in the density functional calculations, we assume that the relation in Eq. (11) between the elastic constants and pressure obtained in the Zwanzig–Mountain formulation (based on general principles for a many-particle system) holds. Using the density dependence of $f(\rho)$ of the DFT calculation, we obtain the corresponding pressure using the relation [32]

$$P = \rho \frac{\partial f}{\partial \rho} - f. \tag{17}$$

For the inhomogeneous solid-like state, the bulk viscosity is obtained in terms of the second derivative of the free energy [38] f per unit volume. To see this, we note that the free energy f of the solid-like state is written in terms of the shear and bulk modulus with the following general formula, which follows from the definition [41]:

$$F = \frac{1}{2} \int d^d C_{ijkl} u_{ij} u_{kl}. \tag{18}$$

Here, the u_{ij} represent the symmetric strain tensors and C_{ijkl} the elastic constants tensor. Being an isotropic symmetric tensor, C_{ijkl} satisfies the relation

$$C_{ijkl} = \lambda \delta_{ij} \delta_{kl} + \mu(\delta_{ik}\delta_{jl} + \delta_{il}\delta_{jk}), \tag{19}$$

where λ and μ are called the Lamé coefficients. Using the above form for the elastic tensor given in Eq. (19), the corresponding free energy for an isotropic inhomogeneous solid is obtained as

$$F = \frac{1}{2} \int d\mathbf{x} \left\{ \lambda' \bar{u}^2 + 2\mu \tilde{u}_{ij} \tilde{u}_{ji} \right\}, \tag{20}$$

where we have substituted $\bar{u} = u_{ii}$ as the trace of the u_{ij} matrix, and $\tilde{u}_{ij} = u_{ij} - \delta_{ij}\bar{u}/d$ is the traceless part of u_{ij}. Here, we have used the Einstein convention of repeated indices being summed over. In Eq. (20), $\lambda' = (\lambda + 2\mu/3)$ and μ respectively denote the bulk and shear muduli of the isotropic

solid. From this expression the bulk modulus is obtained in terms of the second derivative of the free energy density,

$$\lambda + \frac{2\mu}{3} = \rho^2 \frac{\partial^2 f}{\partial \rho^2}, \tag{21}$$

and is obtained from the density dependence of the DFT-value free energy for the metastable state. For the shear modulus μ of the solid we use the relation in Eq. (11) for the high-frequency limit, i.e. $\lambda = \mu + 2(P-1)$, with the pressure P obtained from the DFT result in Eq. (17). The corresponding Poisson ratio ν is obtained in terms of λ and μ as

$$\nu = \frac{\lambda}{2(\lambda + \mu)}. \tag{22}$$

With the calculation of the short-time elastic constants in terms of the Lamé coefficients $\{\lambda, \mu\}$, we obtain the Poisson ratio ν corresponding to a chosen value of the softness index n. To summarize, in the present calculation we have used the free energy for the inhomogeneous system obtained from the density functional methods [38,42,43] and computed the elastic constants in the high-frequency limit.

4. Results and interpretation

We now present the numerical results for the fragility and elastic constants obtained using the models described in the previous sections. The nature of the correlation between these two properties which follows from these results is the primary observation of this work. The first step in this is identification of the metastable state for the liquid with a chosen interaction potential. This is done by minimization of the free energy functional $f[\rho]$ from the appropriate density distribution.

4.1. Free energy with MWDA

Using the inputs outlined in the previous section we identify the metastable state of the liquid as a local minimum of the free energy and calculate the configurational entropy $\mathcal{S}_c$ for the liquid. The density function is characterized with the choice of $\{\mathbf{R}_i\}$ in terms of the pair function $w(r)$ defined in Eq. (15). Figure 3 shows the Bernal pair function $g_B(r)$ vs. r for the hard-sphere system, with r being scaled with respect to the hard-sphere diameter. It should be noted that the pair function $g_B(r)$ represents distribution of the centers of Gaussian density profiles and not that of the actual particles. Thus, for the hard-sphere system the value of $g_B(r)$ is a maximum at a distance $r > \sigma$ and not at the contact. The inset of Fig. 3 shows our choice for the respective variations of the contact value of $w(r = \sigma, n)$, i.e. $w_c(n)$ (see Eq. (16) for the definition) vs. the softness index n. We consider two specific structures as test cases in which the constant c_0 is respectively chosen as 0.02 and 0.08. We refer to these two structures characterized by the respective $w_c(n)$ as structures A and B in the following discussion. These represent otherwise similar structures, differing only at very short length scales $\sim\sigma$. The packing fraction considered is $\eta = 0.60$, and for the scaling parameter introduced in Eq. (15) we choose $\eta_0 = 0.70$.

To demonstrate the DFT calculation, the total free energies amorphous structures A and B are calculated for systems with soft-sphere interaction potential with $n = 25$. The integral equations of MWDA, stated in Eqs. (A.4) and (A.5) of Appendix A, are solved using the input structure factor $c(r)$ for the corresponding equivalent hard-sphere system of diameter d_n. The latter is obtained using the

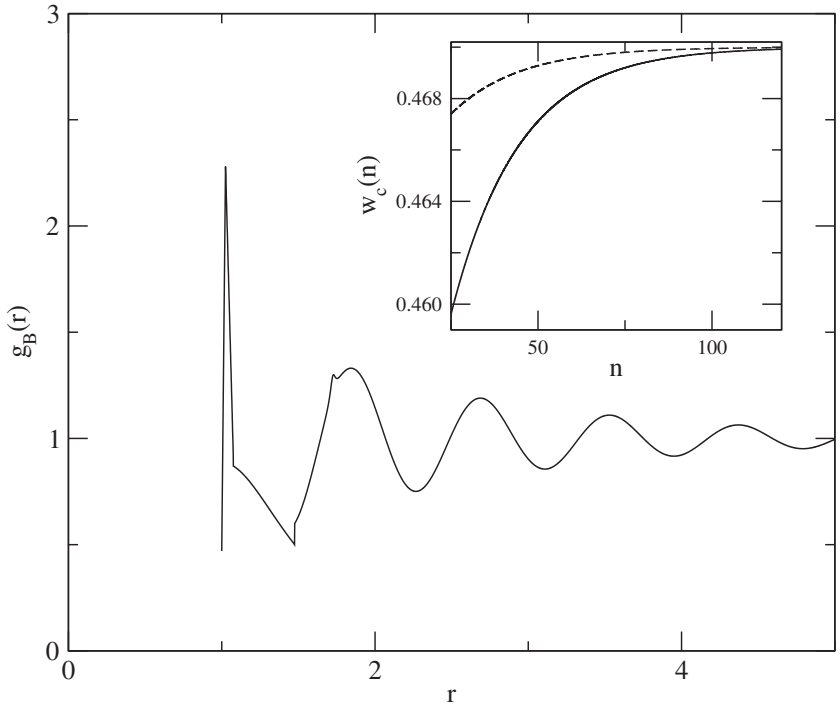

Fig. 3. The Bernal structure function $g_B(r)$ vs. r/σ for the hard-sphere system introduced on the right-hand side of Eq. (15). The inset shows the values of the structure function $w(r, n)$ at closest approach, denoted as $w_c(n)$, vs. the softness index n for the soft-sphere system corresponding to structures A (solid) and B (dashed). For both structures A and B shown in the inset, the packing fraction is $\eta = 0.60$ and the parameter η_0 is chosen as 0.70; $w_c(n)$ is calculated following Eq. (16) with $c_0 = 0.02$ (structure A) and 0.08 (structure B).

Barker–Henderson formula in Eq. (14). The total free energy corresponding to structure A depicted above [for $c_0 = 0.02$ in Eq. (16)] is obtained from Eq. (A.1), and the results for different densities are displayed in the main panel of Fig. 4. The MWDA free energies corresponding to different values of the width parameter α are presented here. The free energy at the minimum represents the corresponding metastable state. For structure A, the density dependence of the optimum width parameter $\alpha_{\min}$ at the free energy minimum is shown in the inset of Fig. 4. How the respective free energies of the metastable states per particle change with the density η is displayed in Fig. 5. We also calculate the free energy of the uniform liquid state (for $\alpha \to 0$) at the same density. Figure 5 shows that for both structures A and B the free energy values are very similar, and both structures become metastable with respect to the uniform liquid state at around the same value of η. While the actual values of the respective total free energies are not very different for the two structures, the variation of the MWDA density of the equivalent liquid, i.e. $\hat{\eta}$, with the softness index n becomes qualitatively different corresponding to those two structures. This difference is displayed in Fig. 6, where we show the variation of the effective liquid density $\hat{\eta}$ with respect to the index n as obtained from calculations done with structures A and B. The main panel and the inset of Fig. 6 respectively show these two cases with qualitatively opposite behaviors. This occurs due to the difference in short-range structures corresponding to the choices of the respective contact values for the pair function $w(r)$ in cases A and B. To summarize the key observations, the correlation between effective fluid density $\hat{\eta}$ and the softness index n of the interaction potential sensitively depends on the short-range amorphous structure for the metastable state.

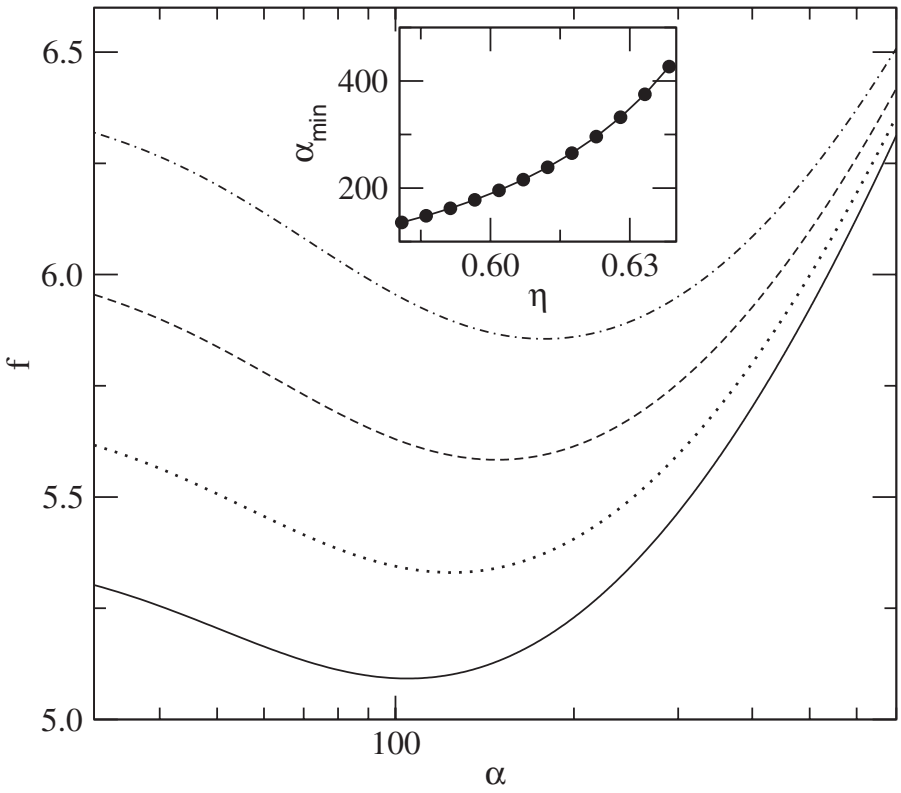

Fig. 4. MWDA free energies vs. α for packing fraction $\eta = 0.565$ (solid), 0.578 (dotted), 0.586 (dashed), and 0.597 (dot-dashed) for soft-sphere interaction with $n = 25$ (main). The inset shows the optimum $\alpha_{\min}$ at the free energy minimum vs. the corresponding η.

4.2. Elastic constants

For the soft-sphere interaction potential characterized by a specific choice of the index n, we follow the procedures for the MWDA outlined above and obtain the free energy of the metastable state as a function of the average density. By calculating numerically the derivatives of $f[\rho]$ with respect to ρ, we obtain the corresponding high-frequency elastic constants from the formulas in Eqs. (17) and (21). The Poisson ratio ν at the corresponding density is calculated using the relation in Eq. (22). These results for ν vs. the softness index n are shown in Fig. 7 for a few different fixed densities and also corresponding to the two chosen structures, A (main panel) and B (inset). The elastic properties and the Poisson ratio are dependent on the density. On the other hand, for a fixed density it becomes essentially independent as the potential becomes very steep with n going beyond 60.

4.3. Thermodynamic fragility

To evaluate the thermodynamic fragility $m_{\rm T}$ as defined in Eq. (6), we calculate the configurational entropy $\mathcal{S}_{\rm c}(\eta)$ as a function of the density η. This also requires the ratio $\Delta_{\rm K} = \eta_{\rm K}/\eta_{\rm g}$ for the corresponding material; $\eta_{\rm K}$ and $\eta_{\rm g}$ are therefore determined by extending the density functional theory to calculate the configurational entropy.

Kauzmann point: The configurational entropy $\mathcal{S}_{\rm c}$ is determined following the steps described in Sect. 2 and Appendix B. The density at which the extrapolated $\mathcal{S}_{\rm c}$ goes to zero marks the Kauzmann point, $\eta_{\rm K}$. As an example, in Fig. 8 we display, for a set of index parameters n of the interaction potential, the η dependence of $\mathcal{S}_{\rm c}$. Here, the chosen value of $w_c(n)$ corresponds to the input

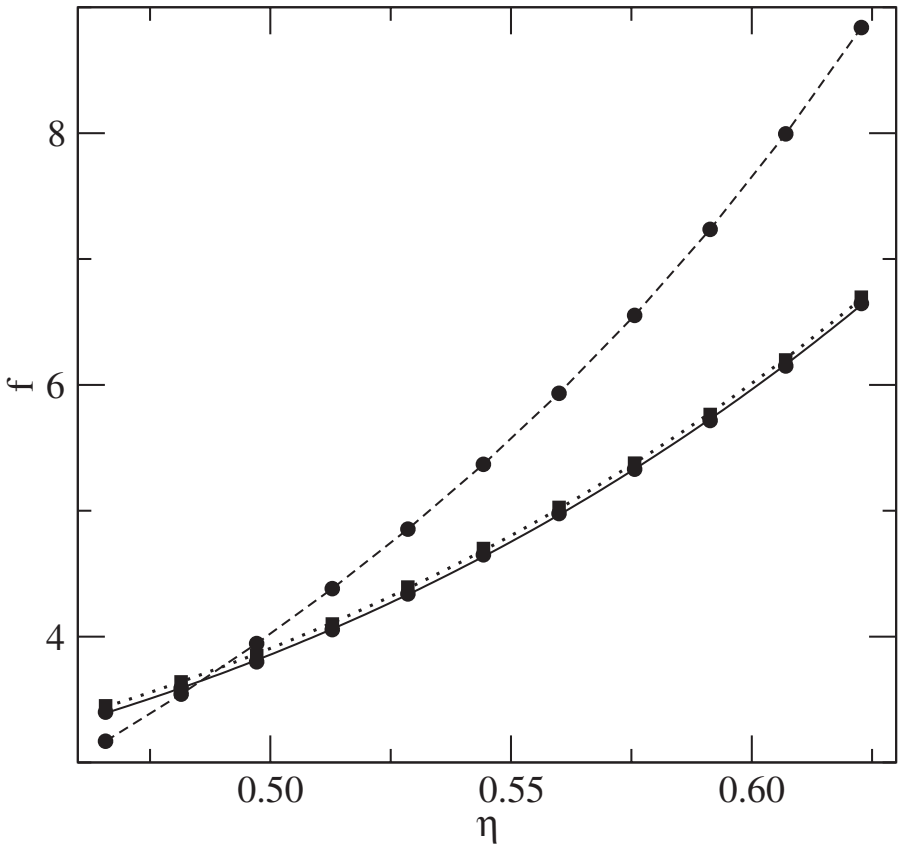

Fig. 5. Free energy f vs. packing η for soft potential index $n = 25$ corresponding to the uniform density liquid state (dashed), structure A (solid), and structure B (dotted).

structure A. The results for $\mathcal{S}_c(\eta)$ shown here are fitted to the form in Eq. (5) and the corresponding packing function η_K is obtained by extrapolation of the $\mathcal{S}_c$ curve. The same calculation is also done for structure B. Variations of the parameters S_0 and η_K on the softness index n of the interaction potential are respectively displayed in Figs. 9 and 10. In these figures, the results corresponding to both structures A (main panel) and B (inset) are shown. The trends observed in the respective dependence S_0 and η_K on the softness index n are reversed as the short-range structure changes from A to B.

Glass transition point η_g: In the present model the glass transition point η_g is defined to be the density at which $\log_{10}[\tau_\alpha/\tau_0]$ reaches a chosen value $\mathcal{B}$—see Eq. (7) in Sect. 2. Using this defining relation, we obtain a transcendental equation for η_g: $\mathcal{S}_c(\eta_g) = a_0\eta_g$. This equation is solved graphically. For this, we first plot the $\mathcal{S}_c(\eta)$ vs. η curve using DFT. The graphical solution of the equation corresponding to $n = 25$ and structure A is displayed in Fig. 11. Note that the determination of both η_K and η_g involves extrapolation of the configurational entropy curve.

With the above-described procedure, we calculate η_K and η_g (and hence Δ_K) corresponding to both the structures A and B depicted above. A key observation that emerges here is that Δ_K's dependence on the softness index n is very sensitive to the short-range structure of the metastable heterogeneous state. Between the two structures A and B depicted above, the dependence of Δ_K on n is reversed. This is displayed in the main panel and inset of Fig. 12. Using the relations given by Eqs. (6) and (7),

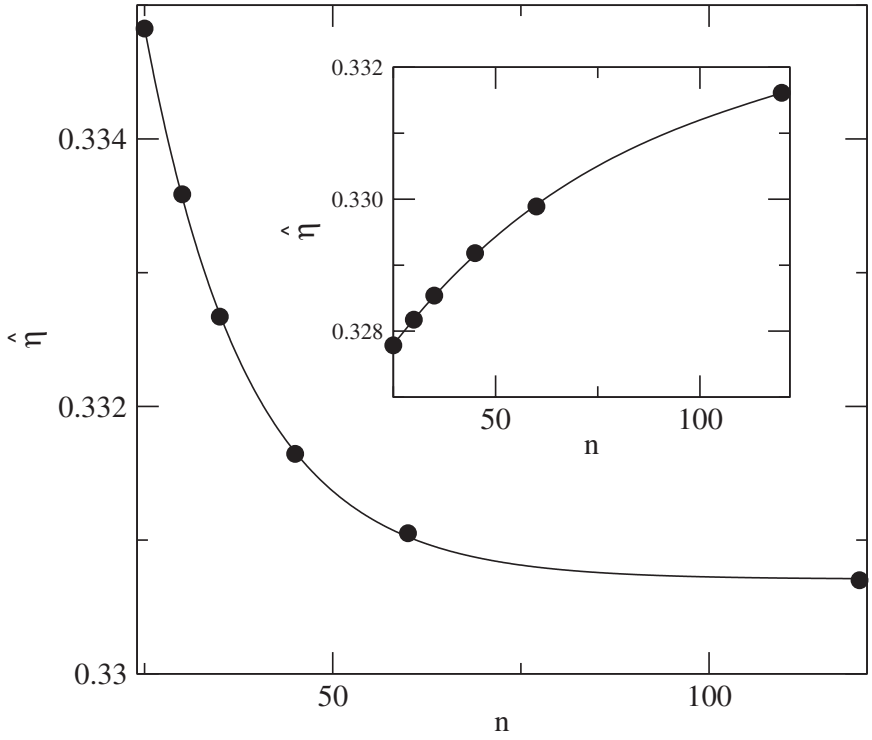

Fig. 6. The packing fraction $\hat{\eta}$ for the effective system of MWDA vs. the soft-sphere potential index n at $\eta = 0.597$. The main figure and inset respectively show the dependence for case A and case B. The slight difference in the short-range structures corresponding to A and B reverses the n dependence of $\hat{\eta}$.

we obtain the following definition for thermodynamic fragility:

$$m_{\mathrm{T}} = \frac{1}{a_0 \eta_{\mathrm{g}}} \left[1 + \frac{a}{\Delta_{\mathrm{K}} - 1} \right]. \tag{23}$$

For a chosen soft-sphere potential with a specific n, the calculation of the configurational entropy $\mathcal{S}_{\mathrm{c}}$ obtains the corresponding values for the exponent a, the density η_{g}, and the ratio Δ_{K}. Hence, the thermodynamic entropy m_{T} is obtained from the formula in Eq. (23). We plot the thermodynamic fragility m_{T} vs. the Poisson ratio ν calculated at $\eta = \eta_{\mathrm{g}}$ for both structures A and B. These results are respectively shown in the main panel and inset of Fig. 13. A key feature of this figure is that on changing from structure A to structure B the correlation between ν and m_{T} changes in a qualitative manner. For structure A, as n is increased the fragility m_{T} increases, starting from a relatively low value for small n. On the other hand, for structure B, in which a larger number of particles are present in the first shell compared to structure A, the fragility m_{T} is already high even at small n, and then falls as the potential gets stiffer with increasing n. As a result, we observe qualitatively opposite correlations between ν and m_{T} for the two structures A and B. Finally, the dependence of m_{T} on n is displayed in Fig. 14. Here also, qualitatively opposite behaviors of the thermodynamic fragility m_{T} with respect to variations of the softness index n are observed for the two structures A and B. In both cases, the same result for m_{T} is obtained in the limit of large n, which represents a hard-sphere potential.

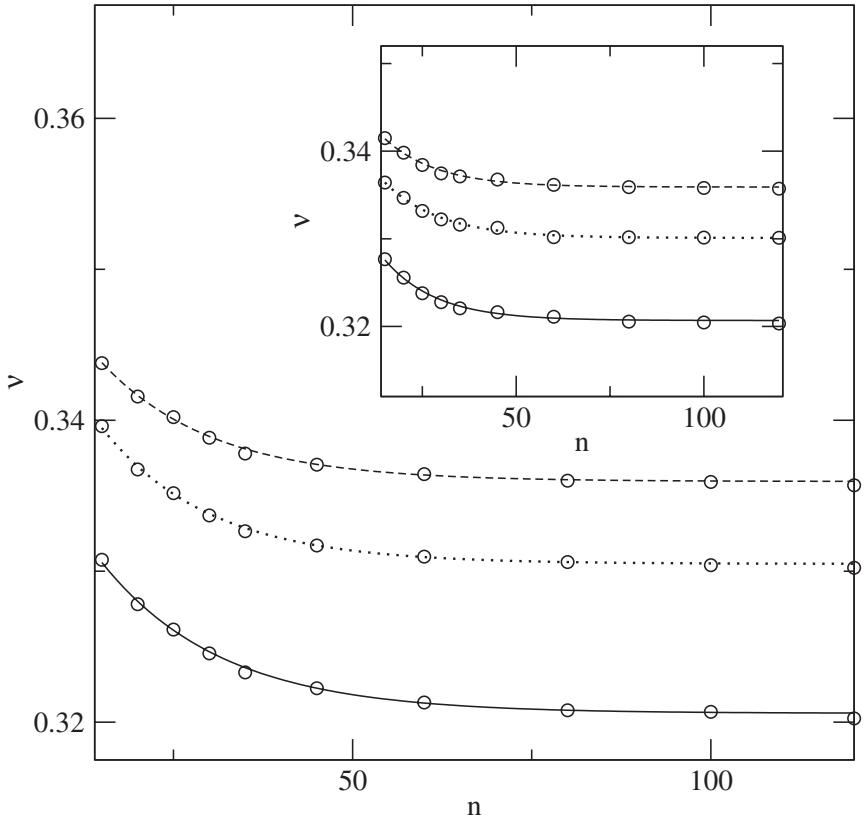

Fig. 7. The ratio v vs. softness index n of the interaction potential for three values of the packing η equal to 0.550 (solid), 0.580 (dotted), and 0.600 (dashed). The main panel (inset) shows the results for structure A (structure B).

5. Discussion

In this paper we have studied how the fragility m_{T} of a metastable soft-sphere liquid depends on the softness index n of the interaction potential between its particles, as defined in Eq. (3). The approach is based on estimating the configurational entropy $\mathcal{S}_{\mathrm{c}}$ of the metastable liquid using the MWDA of classical density functional theory. The calculation involves averaging over an ensemble of aperiodic density distributions representing the metastable liquid state. This is implemented through the use of a pair correlation function $w(r, n)$ for the amorphous structure. We estimate $w(r, n)$ using, as a basis, the Bernal structure for a hard-sphere system and the corresponding pair correlation function $g_{\mathrm{B}}(R)$. Our choice of the Bernel function in this case is not unique, however. Alternatively, information from computer simulations of glassy structures has also been used [64] to present the random lattice, with similar results for the metastable free energy minimum. In some cases [65], the set $\{\mathbf{R}_i\}$ itself has been treated as minimization parameters for the free energy.

The MWDA obtains the free energy of a hard-core system quite accurately in terms of an equivalent uniform low-density fluid. The MWDA approach used here is particularly suitable for hard-sphere systems. Keeping up to second order in density fluctuations, this approximation describes quite accurately hard-core systems in terms of an equivalent uniform low-density fluid. For purely hard-core repulsive systems, no expansion for the Hamiltonian in terms of displacements from equilibrium sites exists. The lattice dynamics is entirely controlled by collisions. Movements of the particles between collisions lose coherence very rapidly. In the solid state, the hard spheres move freely

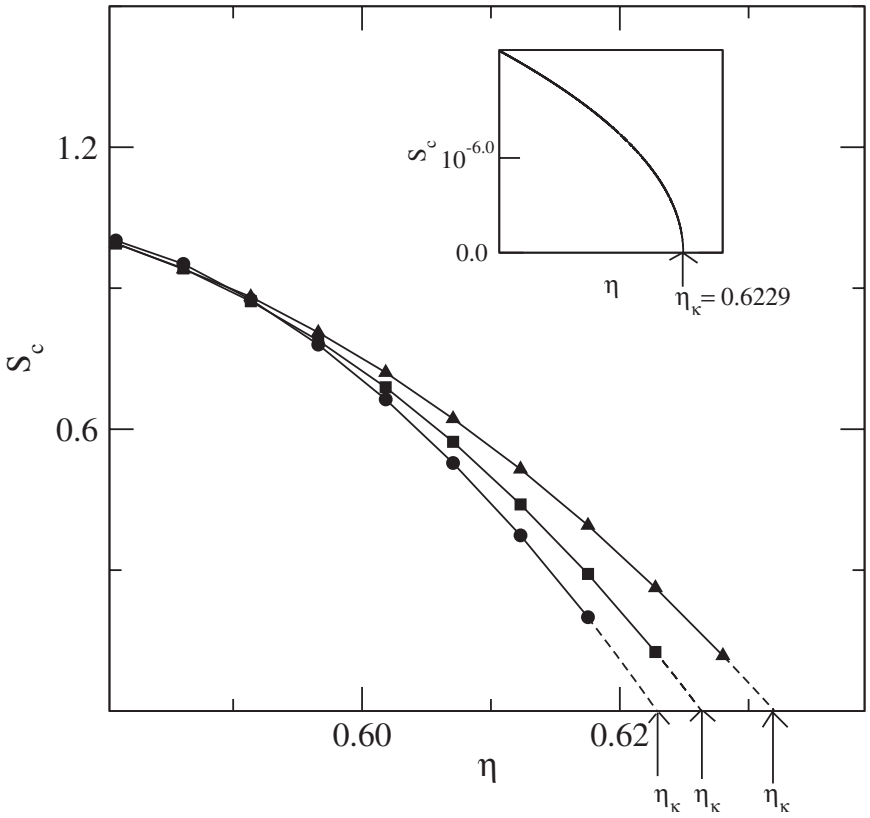

Fig. 8. Configurational entropy $\mathcal{S}_c$ in units of k_B vs. packing for soft-sphere potentials corresponding to $n = 25$ (circles), 30 (squares), and 60 (triangles). The lines show fits of the corresponding data to the formula given in Eq. (5). The respective η_K values for the three curves, shown with arrows, are 0.623, 0.626, and 0.632 with growing n. The variation of the fit parameters S_0 and η_K with the softness index n are respectively shown in Figs. 8 and 9. The inset shows the corresponding behavior of the extrapolated $\mathcal{S}_c$ curve for $n = 25$ in the close vicinity of η_K. All the results for $\mathcal{S}_c$ correspond to structure A.

between collisions and their motion on the average is very much like the constituent particles in the low-density fluid. This method is extended here for a soft-sphere system. However, with increasing softness of the potentials this analogy of mapping to an equivalent liquid is weak. For the $1/r^n$-type potential (where $n \to \infty$ is the hard-sphere potential), as n approaches values more typical of short-range interactions in real systems, the coherence in motion of the particles increases. Therefore, with softer potentials the above similarity between the low-density liquid and the solid is absent, and as a result the weighted density functional theories are less successful in understanding inhomogeneous fluids with softer interactions. In addition, for the hard-sphere crystal the average domain of motion of a particular sphere is constrained in space over a scale determined largely by the range of the direct correlation function $c^{(2)}(r)$ at the corresponding density. Hence, the coarse-graining length scale of the weighted density, over which the inhomogeneous density should be averaged, sharply increases with decreasing n. It would therefore be appropriate to include higher-order correlations like $c^{(3)}$ in the calculation of the weight function for the formulation of DFT for softer potentials. In our study the results for the fragility of soft-sphere interactions with large values for index n approach the corresponding value for a hard-sphere system.

In the DFT models described here, we demonstrate how the liquid's structure influences its long-time dynamics. There is a fundamental link between fragility and elasticity through the basic

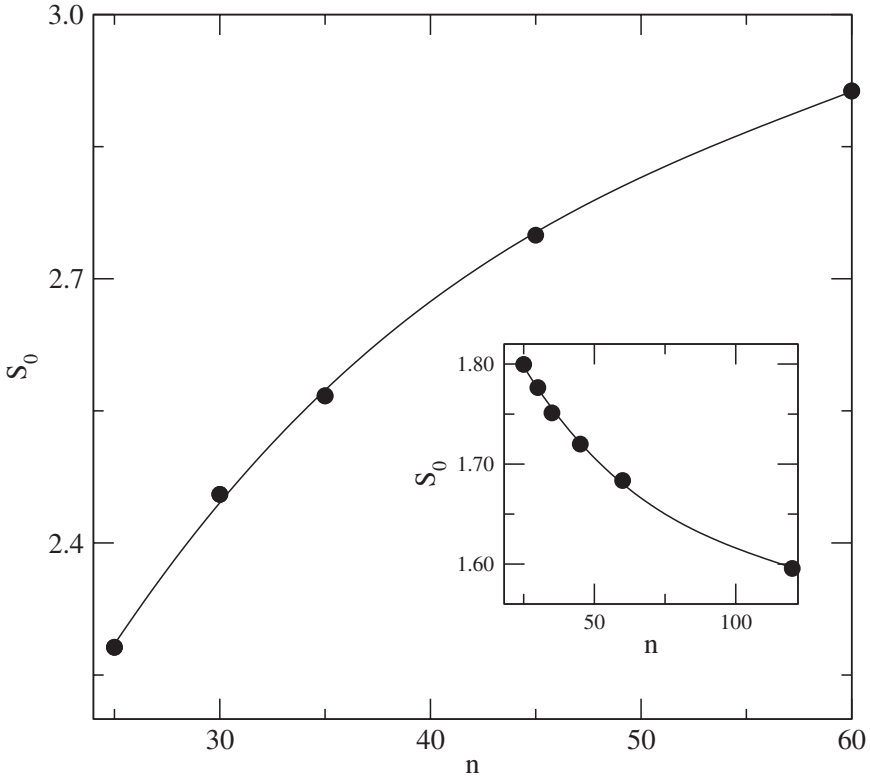

Fig. 9. Parameter S_0 for the formula in Eq. (5) vs. the index n of the soft-sphere potential. The main figure shows S_0 vs. n corresponding to structure A (see text). The same results for structure B are shown in the inset.

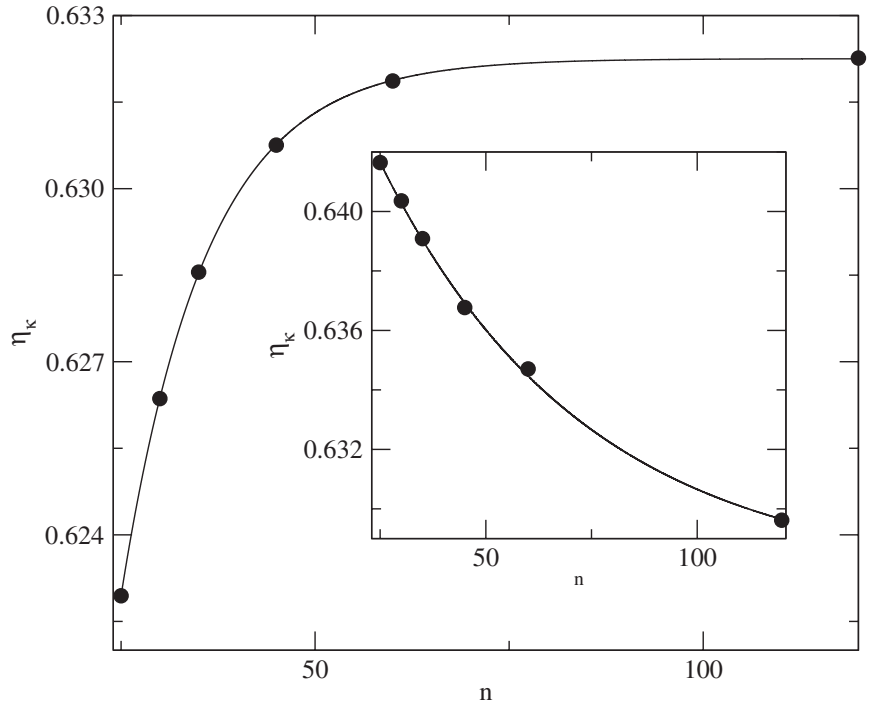

Fig. 10. Parameter η_K for the formula in Eq. (5) vs. the index n of the soft-sphere potential shown in the Main panel for structure A (see text). The same results for structure B are shown in the inset.

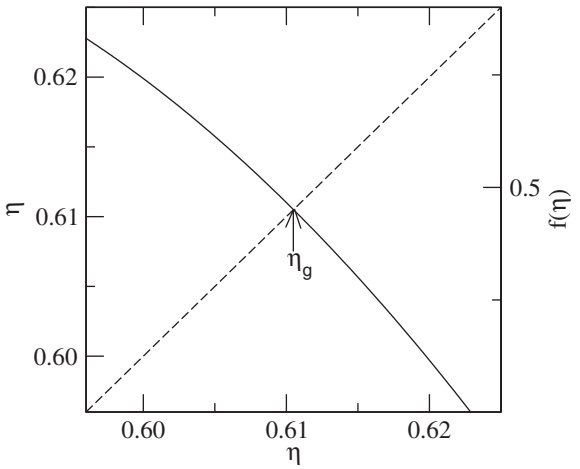

Fig. 11. Graphical solution of transcendental equation $\mathcal{S}_c(\eta_g) = a_0\eta_g$ (see text) at $n = 25$ corresponding to structure A (see text).

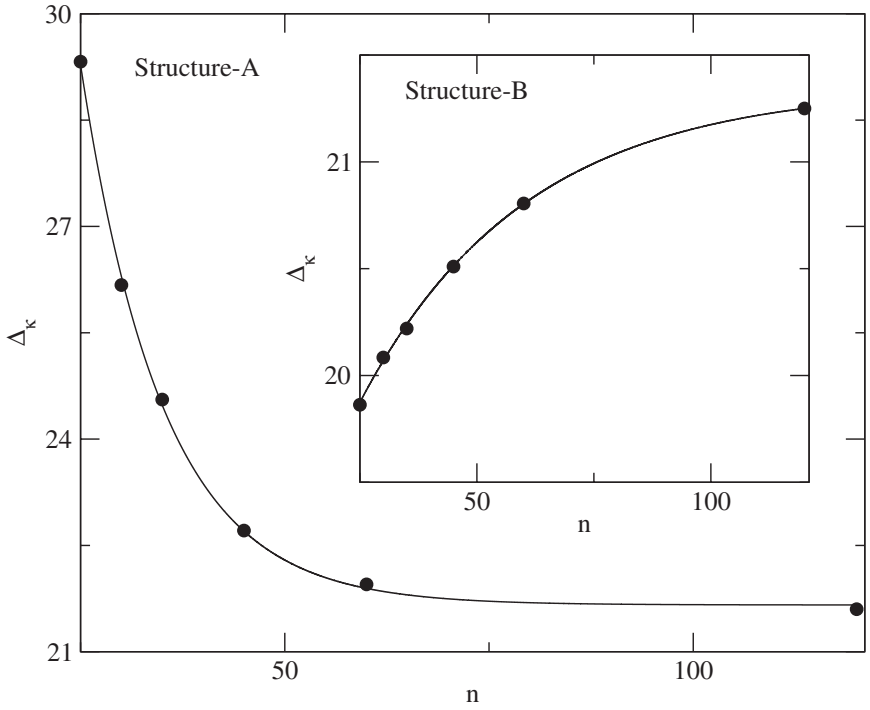

Fig. 12. Δ_K (multiplied by a factor of 10^3) vs. the soft potential index n for structure A (see text). The inset shows the same result for structure B.

interaction potential. Elastic response of a supercooled liquid approaching glass transition signifies solid-like behavior. The fragility index, on the other hand, is related to the relaxation process in the liquid state near the so-called glass transition point. Developing a common basis for both elasticity and fragility at the microscopic level involves understanding the development of rigidity in the ergodic liquid state. The success of basic theoretical models in understanding this rigidity transformation of the metastable liquid into an amorphous solid-like state has only been partial until now. The observed correlation between m and ν demonstrated in the present work is still at the level of a hypothesis. It is also useful to note here that dynamic fragility is generally defined with the

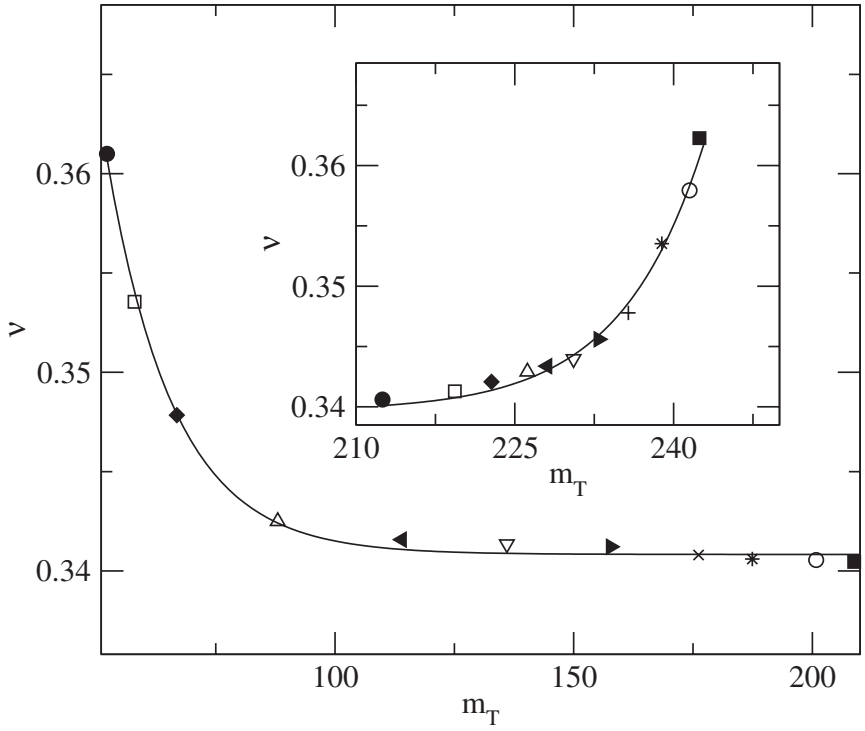

Fig. 13. Poisson's ratio ν vs. the thermodynamic fragility index $m_{\rm T}$ for structures A (main panel) and B (inset). The points in the main panel (inset) with decreasing (increasing) values of $m_{\rm T}$ correspond to interaction potentials with softness index n equal to 120 (filled circle), 60 (open square), 45 (filled diamond), 35 (open triangle up), 30 (filled triangle left), 25 (open triangle down), 20 (filled triangle right), 15 (cross), 10 (star), 8 (open circle), and 5 (filled square). The solid (dashed) line in the main panel (inset) are guides to the eye. The variations of $m_{\rm T}$ with respect to ν for the respective structures A and B show qualitatively opposite trends.

slope of the Angell plot at the temperature $T = T_{\rm g}$. We have defined fragility here through density dependence [7]. This newly defined fragility still correlates with changes in the high-frequency shear modulus or the Poisson ratio.

The key link between the fragility and the structural properties of the metastable liquid relies on the role of configurational entropy in driving a slow dynamics in the supercooled state. Identification of $m_{\rm T}$ as the thermodynamic analogue of fragility in the present context follows from the commonly accepted norm that for a supercooled liquid the fast-growing relaxation time is driven by the fall in its configurational entropy $\mathcal{S}_{\rm c}$. This links two important basic properties of glassy systems, dynamics and thermodynamics. We have shown here that, depending on the short-length-scale structure, both increase and decrease of fragility $m_{\rm T}$ with increasing softness index n is possible. Such opposing trends have also been observed in experimental data on molecular glasses [44–52], as well as in computer models of glassy systems [53,54]. In Ref. [55] it was shown that a change in the composition of bulk metallic glasses result in a correlation between fragility index and Poisson's ratio opposite from the typical result. Reference [55] reports that a change of composition from $Cu_{50}Zr_{50}$ to $(Cu_{50}Zr_{50})_{96}Al_4$ and to $(Cu_{50}Zr_{50})_{90}Al_7Gd_3$ leads to a change of m from 62 to 40 and 30 respectively, while Poisson's ratio (ν) *increases* from 0.359 to 0.369 and 0.373. The present work provides the explanation for such a reversal in the correlation between fragility index and Poisson's ratio starting from a microscopic approach for a model system in which the associated time scales of slow dynamics are not as large as molecular glasses.

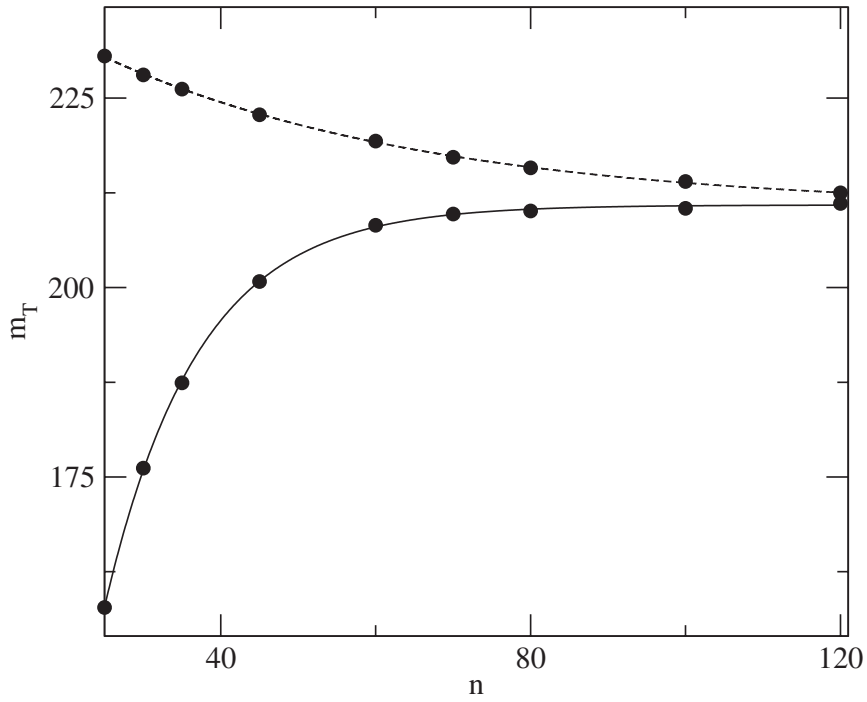

Fig. 14. Thermodynamic fragilty index m_T vs. soft-sphere potential index n, shown with filled circles for structure A (structure B), with a solid (dashed line) shown as a guide to the eye. For the hard-sphere system, the dependence corresponding to the respective structures A and B are qualitatively opposite in trend, both finally converging to a common limit as n becomes large.

Acknowledgements

A. M. acknowledges the University Grants Commission of India for financial support with a UGC-BSR fellowship. S. P. D. acknowledges support under the J. C. Bose fellowship award-grant of Department of Science and Technology, Ministry of Science and Technology, Govt. of India.

Appendix A. Density functional method

We use the MWDA [30] for calculating the free energy of the inhomogeneous liquid in the metastable state. This is an effective medium type approach in which the non-uniform system is mapped to an equivalent homogeneous liquid of lower density. The free energy functional $F[\rho]$ of the liquid is obtained as a sum of two parts,

$$F[\rho] = F_{\rm id}[\rho] + F_{\rm ex}[\rho], \tag{A.1}$$

where $F_{\rm id}$ and $F_{\rm ex}$ respectively denote the ideal gas and the interaction contributions. $F_{\rm id}$ and $F_{\rm ex}$ per particle in units of $\beta(= 1/k_{\rm B}T)$ are respectively denoted as $f_{\rm id}$ and $f_{\rm ex}$. These two free energies are calculated as a functional of the density. For the ideal gas contribution we obtain

$$f_{\rm id}[\rho(\mathbf{r})] = N^{-1} \int d\mathbf{r}\rho(\mathbf{r}) \left(\ln[\rho(\mathbf{r})\Lambda^3] - 1\right). \tag{A.2}$$

Here, Λ is the thermal De Broglie [32] wavelength arising from the momentum integration in the partition function. For large α, corresponding to very localized density distributions, the summation over all lattice sites in $\rho(\mathbf{r})$ is approximated in terms of the contribution from the nearest site, and

Eq. (A.2) reduces to

$$f_{\rm id}(\alpha) \approx -\frac{5}{2} + 3\ln\left(\sqrt{\frac{\alpha}{\pi}}\Lambda\right). \tag{A.3}$$

In the following, Λ and α are scaled in terms of the basic length scale σ (hard-sphere diameter) for the fluid. We denote $\tilde{\Lambda} = \Lambda/\sigma$ and $\alpha^* = \alpha\sigma^2$. We keep $\tilde{\Lambda} = 1.0$ throughout this paper, in line with previous works [28,56].

The MWDA is used to calculate the excess part, $f_{\rm ex}$. The key equation of MWDA [16,57,58] is a self-consistent integral equation [30] involving the weighted density $\hat{\rho}$ or, equivalently, the corresponding packing fraction $\hat{\eta} = \pi\hat{\rho}\sigma^3/6$, in terms of the suitably chosen free energy function $f_{\rm ex}(\hat{\eta})$,

$$\hat{\eta} = \frac{\mathcal{I}(\hat{\eta}, \alpha)}{2f'_{\rm ex}(\hat{\eta}) + \eta f''_{\rm ex}(\hat{\eta})}, \tag{A.4}$$

where the integral $\mathcal{I}$ is

$$\mathcal{I} = N^{-1}\int d\mathbf{x}\int d\mathbf{x}'\rho(\mathbf{x})\rho(\mathbf{x}')c(|\mathbf{x}-\mathbf{x}'|;\hat{\eta}). \tag{A.5}$$

The single and double primes on $f_{\rm ex}(x)$ in Eq. (A.4) respectively denote the first and second derivatives of the function with respect to its argument x. To solve Eq. (A.4), the functional form of the free energy $f_{\rm ex}(\eta)$ is taken from the standard expression of excess free energy of a hard-sphere system [32],

$$f_{\rm ex}(\eta) = \frac{3}{2}\left[\frac{2\eta-\eta^2}{(1-\eta)^2}\right] - \ln(1-\eta). \tag{A.6}$$

The direct correlation function $c(r)$ is obtained in terms of the corresponding Percus–Yevick solution for an equivalent hard-sphere system for the repulsive hard-core potential.

To solve Eq. (A.4) we need to evaluate the integral $\mathcal{I}$ defined in Eq. (A.5), and this requires choosing the set of points $\{\mathbf{R}_i\}$ at which the Gaussian density profiles for $\rho(\mathbf{x})$ are centered. For the free energy evaluation, we average over different choices of this amorphous lattice; the final result is expressed in terms of a pair correlation function $w(r)$ representing the lattice points around which the Gaussian density profiles are centered:

$$\mathcal{I} = -\int d\mathbf{r}_1\int d\mathbf{r}_2\int d\mathbf{R}c(|\mathbf{r}_1-\mathbf{r}_2|;\hat{\eta})\phi(\mathbf{r}_1-\mathbf{R})\phi(\mathbf{r}_2)[\delta(\mathbf{R}) + \frac{6\eta}{\pi}w(R)]. \tag{A.7}$$

Note that $w(r)$ is also dependent on the softness index n.

For a fixed value of η, the total free energy is calculated over a range of values of the width parameter α by solving the MWDA equation in each specific case. Metastable amorphous states, distinct from the uniform liquid state, are identified by locating the intermediate minima of the corresponding free energy with respect to the mass localization parameter α at $\alpha = \alpha_{\rm min}$ for different values of the average packing fraction η. The optimum value $\alpha_{\rm min}$ determines the free energy as well as the optimum density distributions for the equilibrium state. The total free energy $f(\alpha)$ is calculated as a function of the width parameter α. The minimum at $\alpha = \alpha_{\rm min}$ signifies a metastable state, and $\alpha_{\rm min}$ is generally an increasing function of η. The quantity $\ell = 1/\sqrt{\alpha_{\rm min}}$ is the localization parameter

scaled with respect to σ. With increasing η, the particles get more localized and hence the amplitudes of vibration of the particles around their respective mean position fall.

Appendix B. Configurational entropy of the metastable liquid

The configurational entropy $\mathcal{S}_c$ of the amorphous metastable state is obtained here as the difference between the total entropy $\mathcal{S}_{tot}$ and the corresponding vibrational entropy $\mathcal{S}_{vib}$. For $\eta > \eta_F$, where η_F is the freezing point,

$$\mathcal{S}_c = \mathcal{S}_{tot} - \mathcal{S}_{vib}. \tag{B.1}$$

In particular, we focus here on a metastable fluid interaction through a hard-sphere potential. For a hard-sphere fluid [59] the total entropy expressed in units of k_B is

$$\mathcal{S}_{tot} = \frac{3}{2} - f, \tag{B.2}$$

where f is the total free energy. The latter is obtained here by evaluating a functional Taylor expression for the free energy in terms of the density as an order parameter. The vibrational entropy $\mathcal{S}_{vib}$ of the amorphous state is obtained in terms of localized density profiles in a manner similar to the inhomogeneous crystalline state.

The inhomogeneous density $\rho(\mathbf{x})$ is treated as an order parameter for describing the various phases of the liquid [24,41,60]. The density $\rho(\mathbf{x})$ is expressed in terms of localized Gaussian profiles [61] respectively peaked around a set of random points $\{\mathbf{R}_i\}$ constituting an amorphous lattice [62] for the disordered system [25,28,38,63,65]:

$$\rho(\mathbf{r}) = \sum_{i=1}^{N} \left(\frac{\alpha}{\pi}\right)^{\frac{3}{2}} e^{-\alpha|\mathbf{r}-\mathbf{R_i}|^2} \equiv \sum_{i=1}^{N} \phi(\mathbf{r} - \mathbf{R}_i). \tag{B.3}$$

Here, α is the width parameter of the Gaussian function $\phi(\mathbf{r})$. The $\alpha \to 0$ limit corresponds to a uniform liquid, while a large α represents strongly localized density profiles in the inhomogeneous solid. We assume here that the parameter α is the same for every lattice point $\{\mathbf{R}_i\}$ and avoid fluctuations over different sites [66]. The inhomogeneous state with localized density profiles is a solid-like state with elastic behavior [67] and transverse sound modes [68]. The localization of the density profiles gives rise to vibrational modes [69–71]. The crystalline (liquid) state is the most stable state having lowest free energy above (below) the freezing density. For average densities, higher than that corresponding to the freezing point, the free energy functional has local minima for inhomogeneous density functions. These represent states metastable between the liquid and crystalline phases. The strongly heterogeneous states are characterized with amorphous density $\rho(\mathbf{r})$ without any long-range order. To calculate the vibrational entropy $\mathcal{S}_{vib}$ the density profiles are interpreted in a particle analogue. Here, we note that in the DFT model the individual Gaussian density profiles are interpreted as particles vibrating around the respective lattice points $\mathbf{R}_i$. The entropy is reduced due to localization of the particle, as compared to the homogeneous liquid state.

The free energy f involves an ideal gas contribution, which corresponds to a non-interacting system and is written as

$$\mathcal{S}_{id}(\alpha) = \frac{3}{2} - f_{id}(\alpha). \tag{B.4}$$

The ideal gas part of the free energy, $f_{\rm id}(\alpha)$, is obtained for the inhomogeneous system with sharply localized density profiles [61,72]. Let the ideal gas entropies of a non-interacting system in the localized solid-like state and the uniform density liquid state be respectively denoted as $\mathcal{S}_{\rm id}(\alpha)$ and $\mathcal{S}^0_{\rm id}$. The vibrational contribution to the entropy for the amorphous state is obtained as

$$\mathcal{S}_{\rm vib}(\alpha) = \mathcal{S}_{\rm id}(\alpha) - \mathcal{S}^0_{\rm id}. \tag{B.5}$$

Using $\mathcal{S}^0_{\rm id} = 3/2 - f^0_{\rm id}$, where $f^0_{\rm id}$ is the ideal gas free energy of the uniform fluid, the vibrational entropy $\mathcal{S}_{\rm vib}(\alpha)$ is estimated. The above definition of vibrational entropy implies that there is no vibrational contribution to the entropy in the homogeneous state. Using Eqs. (B.2) and (B.5) we obtain that the configurational entropy of the amorphous state corresponding to the mass localization parameter α is

$$\mathcal{S}_{\rm c}(\eta) = \mathcal{S}_{\rm tot}(\eta) - \mathcal{S}_{\rm vib}(\eta) = -(f_{\rm ex} + \ln\eta) + \mathcal{C}_0, \tag{B.6}$$

where $\mathcal{C}_0 = 5/2 + \ln(\pi/6)$. To calculate $\mathcal{S}_{\rm c}$, we need to evaluate the excess free energy $f_{\rm ex}$. This is done here using classical density functional theory. For the inhomogeneous state the free energy is computed using $\rho(\mathbf{r})$ as an order parameter. For large values of the width parameter α, according to Eq. (B.3), the density consists of strongly inhomogeneous profiles. Using Eq. (B.6) we calculate $\mathcal{S}_{\rm c}$.

References

[1] C. A. Angell, Science **267**, 1924 (1995).
[2] R. Böhmer and C. A. Angell, Phys. Rev. B **48**, 5857 (1993).
[3] R. Böhmer and C. A. Angell, Phys. Rev. B **45**, 10091 (1992).
[4] N. Xu, T. K. Haxton, A. J. Liu, and S. R. Nagel, Phys. Rev. Lett. **103**, 245701 (2009).
[5] G. L Hunter and E. R. Weeks, Rep. Prog. Phys. **75**, 066501 (2012).
[6] P. J. Lu and D. A. Weitz, Ann. Rev. Condens. Matt. Phys. **4** 217 (2013).
[7] J. Mattsson, H. M. Wyss, A. Fernandez-Nieves, K. Miyazaki, Z. Hu, D. R. Reichman, and D. A. Weitz, Nature **462**, 83 (2009).
[8] R. Zwanzig and R. D. Mountain, J. Chem. Phys. **43**, 4464 (1965).
[9] R. D. Mountain and R. Zwanzig, J. Chem. Phys. **44**, 2777 (1966).
[10] P. Schofield, Proc. Phys. Soc. **88**, 149 (1966).
[11] J. Boon and S. Yip, *Molecular Hydrodynamics* (Dover, New York, 1991).
[12] C. Kaur, U. Harbola, and S. P. Das, J. Chem. Phys. **123**, 034501 (2005).
[13] P. G. Wolynes, AIP Conf. Proc. **180**, 39 (1988).
[14] G. Adam and J. H. Gibbs, J. Chem. Phys. **43**, 139 (1965).
[15] Y. Singh, Phys. Rep. **207**, 351 (1991).
[16] H. Löwen, Phys. Rep. **237**, 249 (1994).
[17] R. Evans, Adv. Phys. **28**, 143 (1979).
[18] T. Odagaki, J. Phys. Soc. Japan **86**, 082001 (2017).
[19] A. Cavagna, Phys. Rep. **476**, 51 (2009).
[20] L.-M. Martinez and C. A. Angell, Nature, **410**, 663 (2001).
[21] K. Ito, C. T. Moynihan, and C. A. Angell, Nature **398**, 492 (1999).
[22] K. L. Ngai, J. Chem. Phys. **111**, 10403 (1999).
[23] R. J. Speedy, J. Phys. Chem. B **103**, 4060 (1999).
[24] S. P. Das, *Statistical Physics of Liquids at Freezing and Beyond* (Cambridge University Press, New York, 2011).
[25] Y. Singh, J. P. Stoessel, and P. G. Wolynes, Phys. Rev. Lett. **54**, 1059 (1985).
[26] R. W. Hall and P. G. Wolynes, Phys. Rev. Lett. **90**, 085505 (2003).
[27] R. W. Hall and P. G. Wolynes, J. Phys. Chem. B **112**, 301 (2008).

[28] C. Kaur and S. P. Das, Phys. Rev. Lett. **86**, 2062 (2001).
[29] W. A. Curtin and N. W. Ashcroft, Phys. Rev. Lett. **56**, 2775 (1986); **57**, 1192 (1986) [erratum].
[30] A. R. Denton and N. W. Ashcroft, Phys. Rev. A **39**, 4701 (1989).
[31] C. Kaur and S. P. Das, Phys. Rev. E **65**, 026123 (2002).
[32] J.-P. Hansen and I. R. McDonald, *Theory of Simple Liquids* (Elsevier, Amsterdam, 2006), 3rd ed.
[33] J. A. Barker and D. Hendersen, J. Chem. Phys. **47**, 4714 (1967).
[34] J. C. Dyre, Rev. Mod. Phys. **78**, 953 (2006).
[35] F. J. Rogers and D. A. Young, Phys. Rev. A **30**, 999 (1984).
[36] M. D. Carbajal-Tinoco, J. Chem Phys. **128**, 184507 (2008).
[37] J. D. Bernal, Proc. Roy. Soc. London, Ser. A **280**, 299 (1964).
[38] H. Lowen, J. Phys.: Condens. Matter **2**, 8477 (1990).
[39] M. Baus and J.-L. Colot, J. Phys. C: Solid State Phys. **19**, L135 (1986).
[40] C. H. Bennett, J. Appl. Phys. **43**, 2727 (1972).
[41] T. V. Ramakrishnan and M. Yussouff, Phys. Rev. B **19**, 2775 (1979).
[42] M. V. Jarić and U. Mohanty, Phys. Rev. Lett. **59**, 1170 (1987).
[43] M. V. Jarić and U. Mohanty, Phys. Rev. B **37**, 4441 (1988).
[44] M. B. Østergaard, S. R. Hansen, K. Januchta, T. To, S. J. Rzoska, M. Bockowski, M. Bauchy, and M. M. Smedskjaer, Materials **12**, 2439 (2019).
[45] Q. Sun, L. Hu, C. Zhou, H. Zheng, and Y. Yue, J. Chem. Phys. **143**, 164504 (2015).
[46] K. L. Ngai, L.-M. Wang, R. Liu, and W. H. Wang, J. Mol. Liquids **205**, 37 (2015).
[47] W. J. Malfait and C. Sanchez-Valle, Chem. Geol. **346**, 72 (2013).
[48] D. Souri and S. A. Salehizadeh, J. Therm. Analy. Calor. **112**, 689 (2013).
[49] S. V. Nemilov, J. Non Cryst. Solids **353**, 4613 (2007).
[50] V. N. Novikov and A. P. Sokolov, Phys. Rev. B **74**, 064203 (2006).
[51] V. N. Novikov, Y. Ding, and A. P. Sokolov, Phys. Rev. E **71**, 061501 (2005).
[52] C. Dalle-Ferrier, A. Kisliuk, L. Hong, G. Carini Jr., G. Carini, G. D'Angelo, C. Alba-Simionesco, V. N. Novikov, and A. P. Sokolov, J. Chem. Phys. **145**, 154901 (2016).
[53] Z. Shi, P. G. Debenedetti, F. H. Stillinger, and P. Ginart, J. Chem. Phys. **135**, 084513 (2011).
[54] S. Sengupta, F. Vasconcelos, F. Affouard, and S. Sastry, J. Chem. Phys. **135**, 194503 (2011).
[55] K. L. Ngai, L.-M. Wang, R. Liu, and W. H. Wang, J. Chem Phys. **140**, 044511 (2014).
[56] L. Angelani and G. Foffi, J. Phys. Condens. Matt. **19**, 256207 (2007).
[57] Y. Singh, Phys. Rep. **207**, 351 (1991).
[58] N. W. Ashcroft, Aust. J. Phys. **49**, 3 (1996).
[59] A. Mondal, L. Premkumar, and S. P. Das, Phys. Rev E **96**, 012124 (2017).
[60] D. W. Oxtoby and A. D. J. Haymet, J. Chem. Phys. **76**, 6262 (1982).
[61] P. Tarazona, Mol. Phys. **52**, 81 (1984).
[62] S. Torquato, T. M. Tuskett, and P. G. Debenedetti, Phys. Rev. Lett. **84**, 2064 (2000).
[63] C. Dasgupta, Europhys. Lett. **20**, 131 (1992).
[64] K. Kim and T. Munakata, Phys. Rev. E **68**, 021502 (2003).
[65] T. Odagaki, T. Yoshidome, T. Tao, and A. Yoshimori, J. Chem. Phys. **117**, 10151 (2002).
[66] P. Chaudhuri, S. Karmakar, C. Dasgupta, H. R. Krishnamurthy, and A. K. Sood, Phys. Rev. Lett. **95**, 248301 (2005).
[67] S. P. Das and R. Schilling, Phys. Rev. E **50**, 1265 (1994).
[68] R. Ahluwalia and S. P. Das, Phys. Rev. E **57**, 5771 (1998).
[69] S. P. Das, Phys. Rev. E **59**, 3870 (1999).
[70] S. Srivastava and S. P. Das, Phys. Lett. A **286**, 76 (2001).
[71] L. Premkumar, N. Bidhoodi, and S. P. Das, J. Chem. Phys. **144**, 124511 (2016).
[72] P. Tarazona, Phys. Rev. A **31**, 2672 (1985); **32**, 3148 (1985) [erratum].